Characterization of Multiferroic Thin Films Generated with Molecular Beam Epitaxy

Final Report

Margaret Anderson, California Institute of Technology
PI: Darrell Schlom, Cornell University
Mentor: Rachel Steinhardt, Cornell University
Co-Mentor: Katherine Faber, California Institute of Technology

September 17, 2017

Abstract

Magnetoelectric multiferroic thin films exhibit coupled ferromagnetism and ferroelectricity. Interest in these multiferroics stems from their potential applications in spin-based computing and novel information storage methods. Through characterization with x-ray diffraction (XRD), atomic force microscopy (AFM), and vibrating sample magnetometry (VSM), the growth of multiferroic films with molecular beam epitaxy (MBE) was optimized. Both strain-coupled Fe_xGa_{1-x} composites and rare earth ferrite superlattices were studied. Additionally, this study searched for compatible bottom electrodes that facilitate the measurement of the ferroelectric properties of the films. Because the electrodes are necessarily located between the substrate and the film, all three must have compatible crystal lattice parameters in order to grow successfully with MBE. Characterization of the electrodes with XRD omega rocking curves and AFM revealed that PIN-PMN-PT produced slightly better iridium electrodes and Fe_xGa_{1-x} films than PMN-PT.

Introduction

Multiferroic materials exhibit two of ferroelectricity, ferromagnetism, and ferroelasticity [1]. Due to the limited number of materials that fall within this category, the definition is often expanded to include materials that are ferrimagnetic, antiferromagnetic, and other related electric and magnetic properties. While these properties can be combined in numerous ways, this project specifically focuses on magnetoelectric multiferroics. These materials exhibit both ferroelectricity and ferromagnetism [1]. Ferromagnetic materials possess a net magnetic moment and are commonly known as permanent magnets. Ferroelectric materials have a spontaneous polarization resulting from a net dipole moment. Each of these moments can be manipulated by an external field of the same type, electric or magnetic, and even reversed in direction via a 180 degree rotation known as 'switching'. Additionally, the electric and magnetic properties are coupled to one another such that an electric field can theoretically manipulate the magnetic moment within the material through the magnetoelectric effect [2]. The opposite process, magnetic control of the electric dipole moment, is also possible.

The materials with this study are crystalline. They exhibit order on an atomic scale dictated by a basis of atoms organized on a repeating pattern called a bravais lattice. Ferroelectricity is often derived from some form of lattice disorder that causes the electric charges and thereby dipoles within the material to partially align, generating an overall polarization from a net dipole moment. These materials necessarily have a non-centrosymmetric unit cell. Similarly, ferromagnetism arises from the spontaneous alignment of atomic scale magnetic moments, generating a net magnetic moment within the material. The alignment is considered to be the result of super exchange between adjacent atoms. The manipulation of the magnetism via an external field occurs due to the reorientation of preexisting moments rather than the creation of new moments (which is characteristic of diamagnetism).

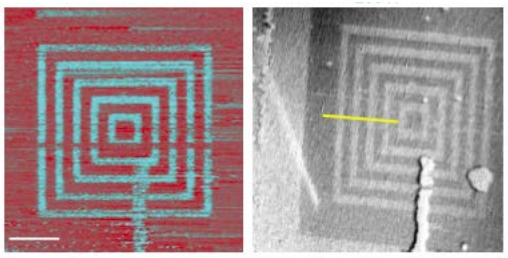

Figure 1: Electrically poled multiferroic film showing coupled electric (left) and magnetic (right) order at 200 K. Coupling persisted at 320 K. Scale bar is 3 μm. Image sourced from Reference 4.

The magnetoelectric coupling of these properties allows several novel device applications for multiferroics. One possibility is low energy computing as spin based devices, as theorized by *Roy et al.* The switching of bits in such a device requires relatively low stress and dissipates a smaller amount

of energy upon scaling, which has been a stumbling block for efforts to miniaturize computing devices. As classical computing components are downsized, energy loss arises from the limited number of electrons that can occupy the material. Thus, it is much more effective to control the device with an electric field, which is not faced with the energy loss of electric current[3]. Additionally, multiferroic devices can be used for memory storage where data is written using local electric fields and read magnetically. These multi-state memory devices eliminate the necessity of large magnetic fields to write data[4]. A proof of concept device was created by Mundy et al. (Fig. 1) which shows the electric control of magnetic moments within a multiferroic thin film. These applications have generated significant research interest in developing high-temperature multiferroics[1]. Ferromagnetic ferroelectric multiferroics were first investigated in the late 1950's. However, early materials were often only multiferroic at low temperatures and thus were impractical for industrial applications. More recently, a few materials have been investigated with promising multiferroic properties at room temperature.

Within the Schlom group at Cornell University, the reactive-oxide molecular beam epitaxy (MBE) growth method is commonly applied to oxides, making them one of the most widely studied classes of materials. While several oxides possess ferroelectric properties, magnetism is harder to achieve. To incorporate magnetic properties within the oxide lattices, transition elements with partially filled d orbitals, including Mn and Fe, are introduced[5]. These elements are associated with magnetic properties within the oxides. Previous research has characterized $BiFeO_3$[6], strained $EuTiO_3$[7], and other materials following the cubic perovskite ABO_3 structure as multiferroics. These examples are all single-phase materials. In contrast, this study examines two multiferroic composites.

The first is considered a strain-coupled composite. The magnetostrictive and body-centered cubic Fe_xGa_{1-x} is combined with a piezoelectric substrate, such as the perovskite $PbMg_{1/3}Nb_{2/3}O_3$-$PbTiO_3$ (PMN-PT), to produce a multiferroic. Piezoelectricity is a phenomena where a dimensional change within the material will induce a change in the external electric field, and vice versa. The structural change is indicative of a change in the lattice constants, or separation of the repeating atomic structure within the crystal. Magnetostriction, on the other hand, results generally from the concept of magnetic anisotropy, where there is a tendency for magnetization to lie in a particular crystallographic direction. When a large externally applied magnetic field attempts to reorient the magnetic moments, a physical strain is produced within the material. The magnetic and electric properties within Fe_xGa_{1-x} thin films are coupled via the transfer of structural strain between the materials. An external electric field generates a mechanical strain within the piezoelectric substrate. This internal strain induces a strain within the Fe_xGa_{1-x} film, leading to a magnetic response via magnetostriction. Therefore, an electric stimulus leads to a magnetic response and vice versa. This study examines single crystal films produced with MBE. In contrast, previous research with Fe_xGa_{1-x} films was limited to polycrystalline samples[8].

The second system utilizes another method of developing materials with coupled electric and magnetic properties: superlattices. This study builds off the work of Mundy et al. with rare-earth ferrite superlattices. In contrast to the highly structured films examined in the 2016 paper, this work characterizes disordered superlattices of hexagonal $LuFeO_3$ and $LuFe_2O_4$. Though pure $LuFe_2O_4$ was once thought to be potentially multiferroic, in depth characterization revealed that the ferroelectric properties were due to regions off-stoichiometry and pure $LuFe_2O_4$ is solely ferrimagnetic[9]. In contrast to the cubic perovskites studied before, ferroelectric $LuFeO_3$ is hexagonal, with a crystal structure compatible with $LuFe_2O_4$. When both phases are combined, the result is a magnetoelectric multiferroic with coupling that is known to persist at room temperature[4].

Through a variety of characterization methods, the growth of thin film samples with MBE was examined. For the $LuFeO_3$/$LuFe_2O_4$ superlattices, the ratio of each phase was determined with X-ray Diffraction. Additionally, the growth of Fe_3O_4 and $NiFe_2O_4$ on top of lutetium ferrite was characterized to determine whether these high Curie temperature materials are good candidates for future multiferroic superlattices. Unfortunately, neither material grew successfully, casting doubt on their compatibility with $LuFeO_3$. By comparing the crystalline quality of electrode and Fe_xGa_{1-x} films, $PbIn_{1/2}Nb_{1/2}O_3$-$PbMg_{1/3}Nb_{2/3}O_3$-$PbTiO_3$ (PIN-PMN-PT) and PMN-PT are essentially equivalent with Ir electrodes and Pt may be a better bottom electrode candidate than Ir. Finally, the ferromagnetic properties of an Fe_xGa_{1-x} film on PMN-PT agreed with the expected results.

Results

The composition of disordered ferrite superlattices was probed with X-ray Diffraction (XRD). θ-2θ scans verified the phases present in each sample. The position and splitting of a diffraction peak around 2θ = 10-20 degrees depends on the ratio of $LuFeO_3$ to $LuFe_2O_4$. Figure 2 shows data for disordered superlattice samples from this summer.

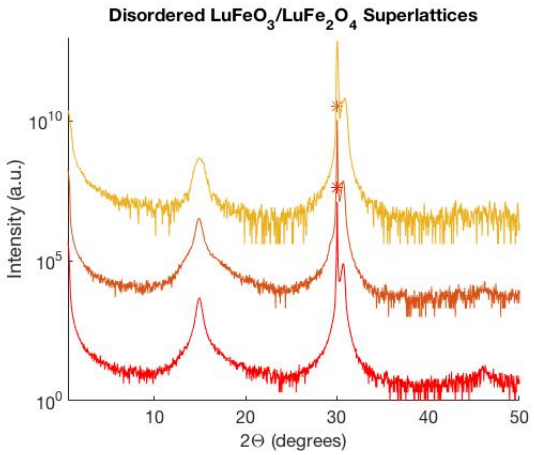

Figure 2: XRD θ-2θ scans of $LuFeO_3$/$LuFe_2O_4$ disordered superlattices grown on YSZ (111) with a Lu:Fe flux ratio between 1:1.1 and 1:1.19 indicated by the position of the single peak around 15 degrees. Substrate peaks are indicated by an asterisk.

When compared to previously collected data (Fig. 3), the

single peak located near 15 degrees indicates a Lu:Fe flux ratio between 1:1.1 and 1:1.19. The superlattices in figure 3 were grown on Ge doped In_2O_3, which results in substrate peaks different from those in figure 2.

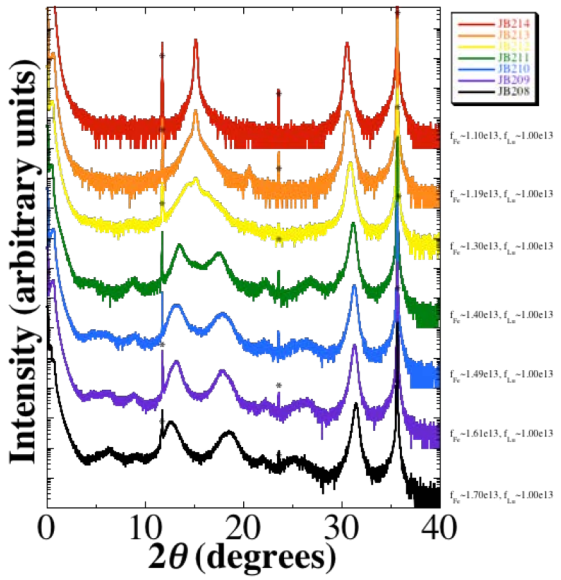

Figure 3: θ-2θ x-ray diffraction scans of disordered lutetium ferrite superlattices on Ge doped In_2O_3 with a range of Lu:Fe flux ratios. The peaks in Figure 2 indicate that the samples have Lu:Fe ratio inbetween the red and yellow curves in this figure. Figure courtesy of Rachel Steinhardt.

While $LuFe_2O_4/LuFeO_3$ superlattices are very successful high-temperature multiferroics, $LuFe_2O_4$ is only magnetic to just below room temperature. At higher temperatures, the thermal energy overcomes the coupling between dipole moments in the material and it undergoes a paramagnetic transition. This transition temperature is called the Curie Temperature of the material. In an attempt to improve the magnetic and therefore multiferroic properties of the superlattices, $LuFe_2O_4$ can be replaced with materials with higher curie temperatures. Both of the cubic spinels Fe_3O_4 and $NiFe_2O_4$ have curie temperatures far above room temperature, making them ideal candidates for multiferroic superlattices. While these two materials have the potential to raise the temperature at which multiferroic properties exist, they must be structurally compatible with $LuFeO_3$.

The compatibility of $LuFeO_3$ with $NiFe_2O_4$ and Fe_3O_4 was evaluated by attempting to grow a layer of the candidate material on top of a $LuFeO_3$ film. The goal was to produce a smooth, flat layer of the material in the desired phase. To determine whether the surface layer was able to grow smoothly, the surfaces were characterized with atomic force microscopy (AFM). AFM is a method of scanning probe microscopy that uses the change in amplitude of an oscillating cantilever to map the topological surface of the sample. If a smooth layer was grown, an XRD θ-2θ scan checked for the proper phase of the material.

For the first sample, a $LuFeO_3$ film was grown on YSZ (111) and capped with a layer of Fe_3O_4. Unfortunately, when imaged with AFM, the Fe_3O_4 was present as triangular islands, rather than the theoretically flat and smooth layer. Topological line profiles of the surface showed an average island height of about 20 nm and a width of 200-300 nm. Because these islands cover about 10 percent of the film surface, it can concluded that the islands are formed from Fe_3O_4 atop a smooth layer of $LuFeO_3$.

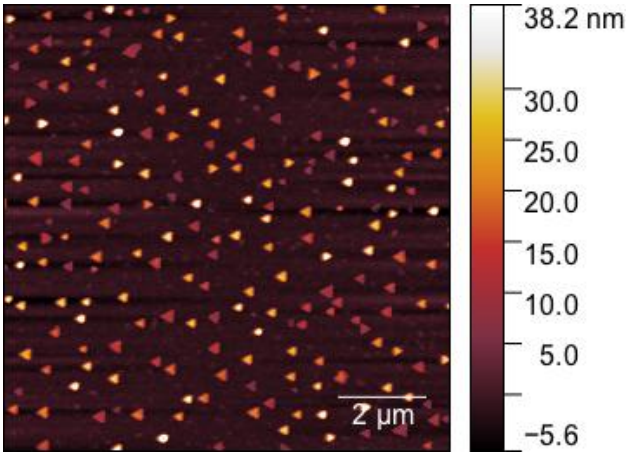

Figure 4: AFM image of an Fe_3O_4 layer on $LuFeO_3$ grown on a YSZ (111) substrate. RMS Roughness of surface excluding islands: 1.036 nm.

Next, a layer of $NiFe_2O_4$ was attempted on $LuFeO_3$. As depicted in the 3D image in Figure 5, the surface of the sample is extremely smooth. The RMS roughness for the surface is 216.2 pm, within the resolution of the AFM. This would be encouraging if the surface was actually $NiFe_2O_4$.

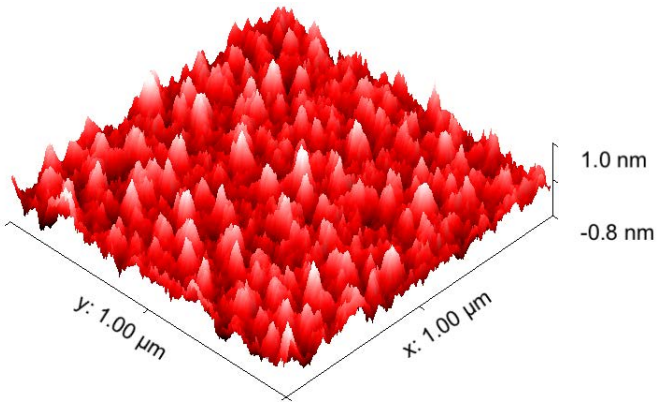

Figure 5: A 3D representation of an AFM scan of the ultrasmooth $LuFeO_3$ on YSZ (111). A layer of $NiFe_2O_4$ was deposited on top of the $LuFeO_3$. RMS surface roughness: 216.2 pm.

When analyzed with XRD (Fig. 6), the data shows a peak for the $LuFeO_3$, but nothing else. Even though the $NiFe_2O_4$ layer was relatively thin and composed of light elements, a broad peak would still be expected. Therefore, it appears the layer grew amorphous rather than crystalline.

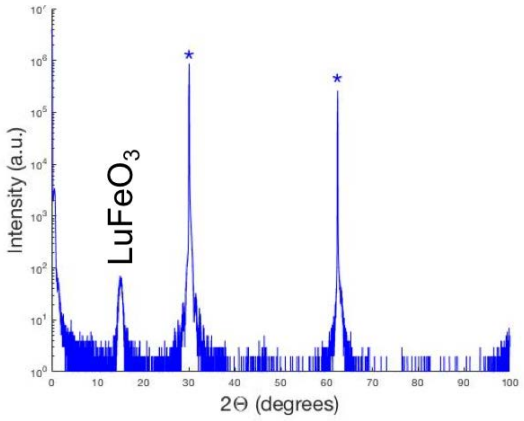

Figure 6: XRD θ-2θ scan of a $LuFeO_3$ film on YSZ (111). The sample was theoretically capped with a crystalline layer of $NiFe_2O_4$, but this data only shows the 0001 peak of $LuFeO_3$ and the expected substrate peaks, suggesting the $NiFe_2O_4$ grew amorphously.

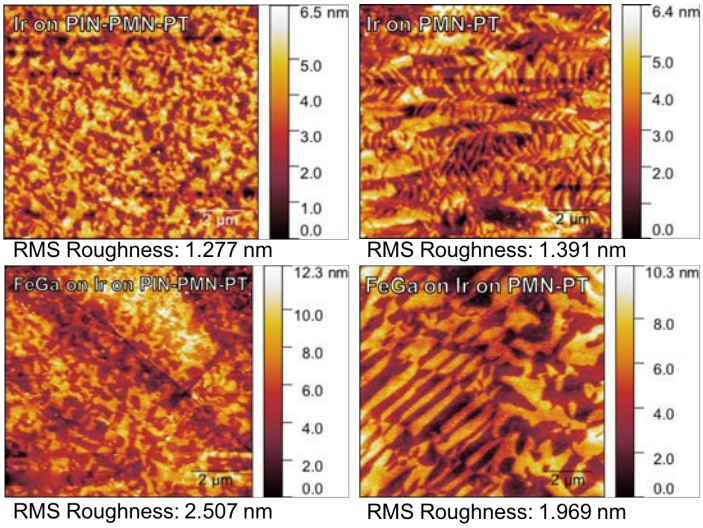

Figure 7: AFM images of 10 μm regions of sample surfaces. The top two images show bare Ir electrodes on a substrate and the bottom images show Fe_xGa_{1-x} films on Ir electrodes on a substrate. The left images are on PIN-PMN-PT substrates and the right are PMN-PT. The average RMS Roughness of the given sample is reported below each image. The color scale to the right of each image shows how the color of the image corresponds with the height variations of the image.

The second half of this study examined Fe_xGa_{1-x} single crystal thin films. The overarching goal was to find a compatible bottom electrode to more effectively measure the ferroelectric properties of the film. The electrode is necessarily located between the substrate and the film. Due to its position, the crystal structure of all three materials (substrate, electrode, and film) must be compatible to grow epitaxially.

The first electrode candidate was iridium. Face-centered cubic Ir was grown on two different substrates known to be compatible with Fe_xGa_{1-x} films: PIN-PMN-PT and PMN-PT. Both of these substrates are variations on pure $PbTiO_3$ with different elements substituted and added to create an increasingly complex unit cell and enhanced piezoelectricity.

To evaluate the quality of film growth, the surface of each film was analyzed with AFM and the RMS roughness was compared. Figure 7 shows AFM images of Ir electrodes on PIN-PMN-PT and PMN-PT and Fe_xGa_{1-x} films on Ir electrodes on each substrate. The average RMS roughness for each sample is recorded below the image. When the RMS roughness data is compared (Fig. 8), the bare Ir electrodes on each substrate have approximately equivalent roughness. When an Fe_xGa_{1-x} film is grown on an Ir electrode on each substrate, the roughness is larger than that of the bare Ir electrodes and slightly larger for PIN-PMN-PT. However, the difference between the Fe_xGa_{1-x} film samples may also be the result of different Fe seed layer thicknesses. The PIN-PMN-PT sample had a 1 nm Fe seed layer thickness, while the PMN-PT sample had a 3 nm thickness. This difference obfuscates the result and limits the ability to use the surface roughness of these samples as an indication of the quality of the film.

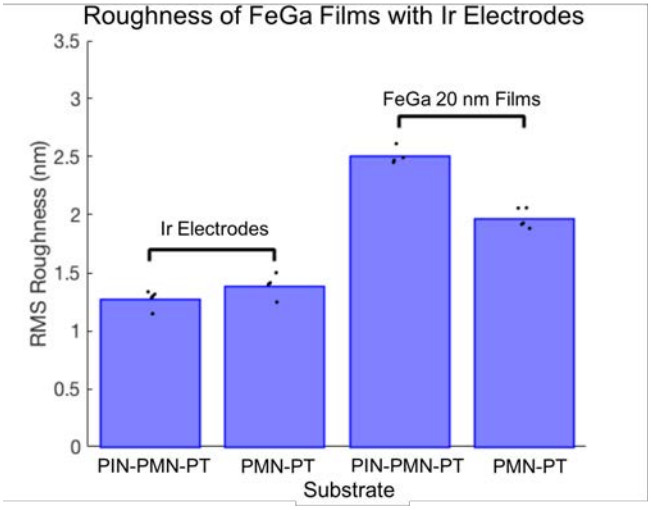

Figure 8: A chart that compares the RMS roughness data from Ir electrodes on PIN-PMN-PT and PMN-PT and Fe_xGa_{1-x} films on Ir electrodes on both substrates. The blue bars indicate the average roughness of the sample. The small black points indicate the individual data points used to calculate the average. The bare Ir electrodes on each substrate (left two bars) have approximately equal roughness. The Fe_xGa_{1-x} film on an Ir electrode on PIN-PMN-PT (second from the right bar) has a slightly higher roughness than on PMN-PT (rightmost bar). While this may be due to higher quality film growth, these samples had slightly different Fe seed layer thicknesses that could affect the roughness values.

With a similar face-centered cubic crystal structure, Pt was also investigated as a potential bottom electrode. A bare Pt electrode was grown on PIN-PMN-PT and an Fe_xGa_{1-x} film was grown on an Pt electrode on PIN-PMN-PT. Figure 9

shows an AFM image of a 10 μm region of the Fe_xGa_{1-x} film sample just described. The average RMS roughness of this sample is 1.205 nm, lower than the equivalent roughness for Fe_xGa_{1-x} films on Ir electrodes on either substrate, especially PIN-PMN-PT.

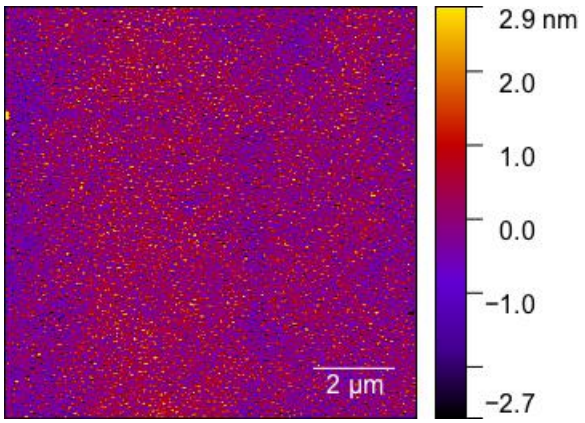

Figure 9: An AFM image of a 10 μm region of a Fe_xGa_{1-x} film on a Pt electrode on PIN-PMN-PT. Average sample RMS roughness: 1.205 nm.

Because the RMS roughness of each sample is an incomplete indication of crystal quality, the internal structural quality of the crystal was evaluated with ω-rocking curves. The full width at half maximum (FWHM) of the peak corresponds to the quality of the crystal. A smaller FWHM indicates a higher quality crystal with a FWHM of nearly 0 indicating a perfect crystal. In reality, small defects within the crystal broaden the peak. The minimum FWHM of a film is that of the substrate because defects within the substrate will necessarily be adopted by the thin film. For that reason, the ω-rocking curve of the film is overlaid on that of the substrate for a more direct comparison. Comparing figures 10 to 12, the FWHM for Ir on PIN-PMN-PT is essentially equivalent to Ir on PMN-PT. This agrees with the surface RMS roughness data from above. Figure 12 shows the ω-rocking curve of Pt on PIN-PMN-PT and gives a FWHM that is less than that of either Ir sample, also in agreement with roughness data.

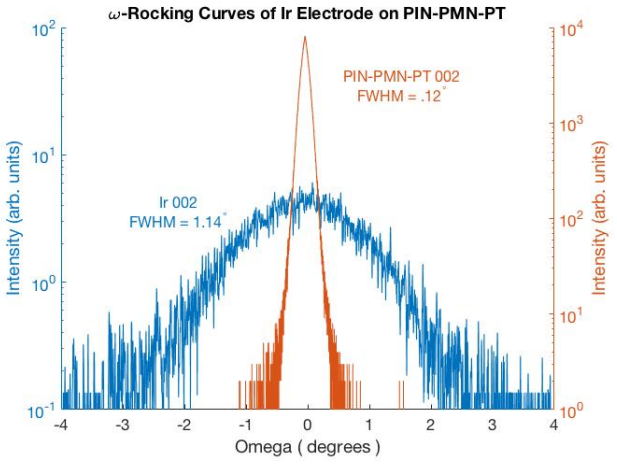

Figure 10: XRD ω-rocking curve of the (002) peak of an Ir electrode (15 nm thickness) on PIN-PMN-PT. The FWHM of PIN-PMN-PT (orange) is 0.1152 degrees. The FWHM of the Ir electrode (blue) is 1.1408 degrees. The y-axis is scaled independently for each curve.

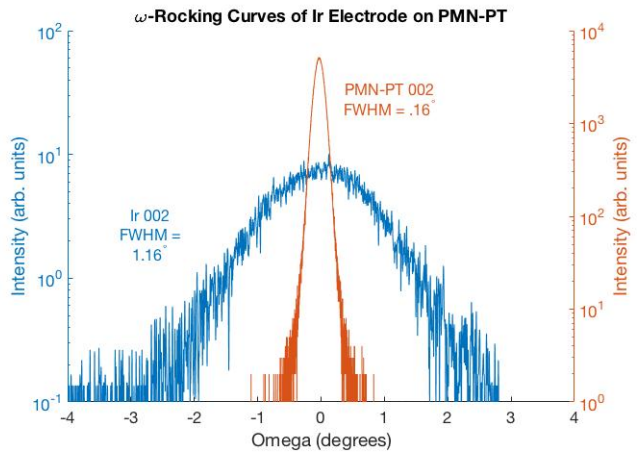

Figure 11: XRD ω-rocking curve of the (002) peak of an Ir electrode (15 nm thickness) on PIN-PMN-PT. The FWHM of PMN-PT (orange) is 0.1624 degrees. The FWHM of the Ir electrode (blue) is 1.1600 degrees. The y-axis is scaled independently for each curve.

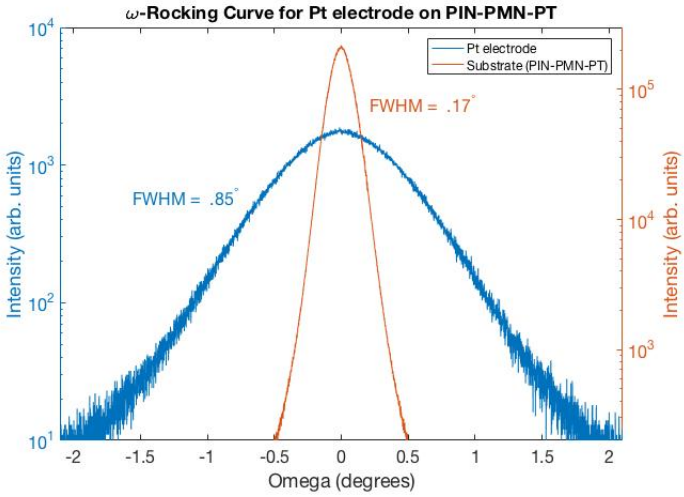

Figure 12: XRD ω-rocking curve of the 002 peak of a Pt electrode (15 nm thickness) on PIN-PMN-PT. The FWHM of PIN-PMN-PT (orange) is 0.1736 degrees. The FWHM of the Pt electrode (blue) is 0.8547 degrees. The y-axis is scaled independently for each curve.

Finally, the magnetic properties of an Fe_xGa_{1-x} film was investigated with vibrating sample magnetometry. By measuring the magnetic response of the sample vibrated in a sweeping external magnetic field, a magnetic hysteresis loop is generated. The loop is characteristic of the in-plane crystallographic direction. Though the vibrating sample magnetometer broke down before characterizing multiple samples, the hysteresis loops of an Fe_xGa_{1-x} film on PMN-PT is shown below. The slightly smaller width of the loop measured in the $\langle 100 \rangle$ direction indicates that it has a slightly smaller coercive field than the $\langle 110 \rangle$ direction. The steeper slope of the purple $\langle 110 \rangle$ loop suggests that the film is easier to magnetize in that direction. These observations agree with previous data from similar films.

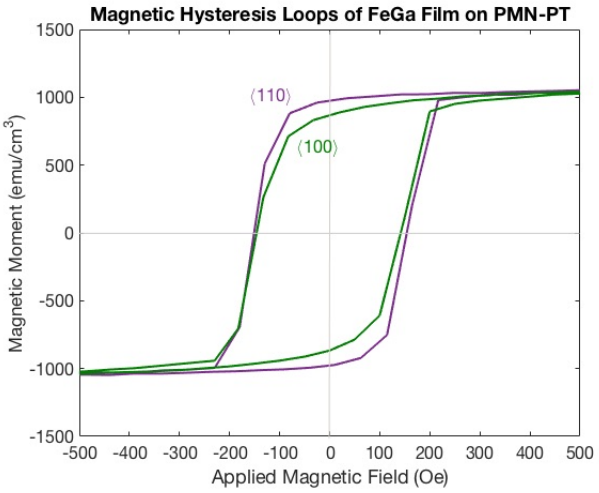

Figure 13: Magnetic hysteresis loops for Fe_xGa_{1-x} films on PMN-PT in the ⟨100⟩ and ⟨110⟩ crystallographic directions. The smaller width of the green loop indicates that the ⟨100⟩ is slightly easier to switch the magnetization.

Discussion

The main focus of research in multiferroics is to produce materials that maintain their electric and magnetic properties beyond room temperature. Electric and magnetic coupling at these high temperatures would facilitate the use of multiferroics in consumer-level device applications. Building off the work of Mundy et al., who produced some of the highest temperature mulitferroic films to date, this project sought to expand the characterization of rare-earth ferrite superlattice films.

$LuFe_2O_4$ is ferrimagnetic up to a transition temperature of about 240 K, slightly below room temperature. Although the magnetic properties persist up to room temperature when composed with $LuFeO_3$ in a superlattice, compounds with higher Curie temperatures could potentially result in higher temperature multiferroic superlattices. This project therefore investigated Fe_3O_4, with a curie temperature of 856 K, and the spinel $NiFe_2O_4$, with a curie temperature of 865 K. Both of these materials are ferromagnetic well above room temperature and therefore are candidates for multiferroic superlattices with ferroelectric $LuFeO_3$. This project investigated the compatibility of these materials with $LuFeO_3$ with the result that neither has the potential to form superlattices in the current growth positions. Fe_3O_4 clumped together to form triangular islands (Fig. 4) and the incredibly smooth surface of the $NiFe_2O_4$ layer (Fig. 5) suggests that it grew amorphously. Unfortunately, neither candidate grew in a smooth regular layer that would support its structural compatibility with $LuFeO_3$.

Previous research presented highly ordered lutetium ferrite superlattices with a highly controlled repeating layered structure (i.e. 9 layers of $LuFeO_3$ and 1 layer of $LuFe_2O_4$). If superlattice films are ever mass produced for device applications, it is unlikely that their growth would be as closely controlled as MBE. Therefore, disordered $LuFeO_3/LuFe_2O_4$ superlattices were investigated in this study. Subsequent investigation revealed that the multiferroic properties of the films relied less on the exact structure of the film and more on the ratio of each phase. Thus, this study investigated the control over composition of the films with a constant Fe:Lu flux ratio during growth. While the film may have regions with 6 layers of $LuFeO_3$ before 1 layer of $LuFe_2O_4$ or 12 layers of $LuFeO_3$, the average composition can remain at a controlled $LuFeO_3$:$LuFe_2O_4$ ratio and still have multiferroic properties comparable to the highly ordered films. The XRD plots in Figure 2 demonstrate the compositional control of the superlattices.

The goal of investigating $Fe_{1-x}Ga_x$ alloys was to find a bottom electrode to facilitate the measurement of ferroelectric properties of the films and more closely mimic the structure of a device made of the films. Though the roughness and ω-rocking curve data shows an inconclusive difference between the substrates PIN-PMN-PT and PMN-PT, the Pt electrode outperformed the Ir in both cases. In reality, the Pt was grown in the presence of oxygen acting as a surfactant, following a suggestion from literature to produce higher quality films. Future research could investigate this growth condition applied to the Ir electrodes and evaluate whether the resulting film quality improves.

Because only one film was characterized with VSM, as a result of an equipment breakdown, future research could examine how the strutural and surface quality of Fe_xGa_{1-x} samples affects the magnetic properties. Future research can also investigate other substrate, bottom electrode, and high Curie temperature $LuFeO_3$ superlattice candidates. Novel composites including out of plane layered materials remain an open field of new research. The future of multiferroic materials is bright, drawing significant new interest with every temperature milestone. In the not so distant future, devices containing multiferroic components could be released to consumers, fueling a further decrease in the energy needed to operate computers and the development of non-volatile memory that persists when power is lost.

Methods

X-ray Diffraction

X-ray diffraction was conducted with a Rigaku Smartlab X-ray Diffractometer with a Ge 220 monochrometer on the incident side in a parallel beam (PB) configuration. Samples were placed on misoriented single crystal silicon during scanning to limit the background signal. θ-2θ scans were used to verify composition, phase, and orientation of the epitaxial thin films. Based on Bragg's law, x-rays incident on the crystalline sample at a Bragg angle (determined by the presence and separation of crystal planes within the material) diffract with a relative displacement equal to an integer multiple of their wavelength. As a result, the x-rays interact with constructive interference, producing a peak in a θ-2θ scan at the Bragg angle. ω-rocking curves gave a measure of structural crystal quality. By 'rocking' the incident angle of the X-rays near a Bragg angle in XRD, the width of a peak can give an indication of the quality of the crystal. If the crystal was absolutely perfect, the rocking curve would have a FWHM of nearly 0 degrees. The only angle that would satisfy Bragg's law and diffract X-rays would be the exact Bragg angle. How-

ever, defects within the crystal introduce slight changes in the orientation of the crystal planes and diffract x-rays at angles slightly off from the exact Bragg angle of a theoretically pure crystal, thereby widening the peak. Therefore, by performing rocking curve measurements, the structural quality of crystal samples can be determined by the FWHM of the resulting peak.

Atomic Force Microscopy

An Asylum Research MFP-3D scanning probe microscope system in AC tapping mode was used to evaluate the surface quality of samples. AFM uses the change in amplitude of a harmonically oscillating cantilever to map the surface features of a sample. The calculated height of the sample at each position is represented as a colored pixel and arranged spatially to produce an image of the surface. RMS surface roughness, a measure of the average deviation of the film surface from a perfectly flat plane, was used to evaluate the smoothness of film growth.

Vibrating Sample Magnetometry

A 9T Quantum Design Physical Property Measurement System (PPMS) with a vibrating sample magnetometer was used to evaluate the magnetic properties of Fe_xGa_{1-x} thin films. Measurements were conducted at room temperature. By oscillating the sample in a sweeping external magnetic field, a hysteresis loop characteristic of ferromagnetic materials was generated. The raw data was the summation of the magnetic signal from both the sample and the diamagnetic substrate. The result is the sloped loop shown below in Figure 14.

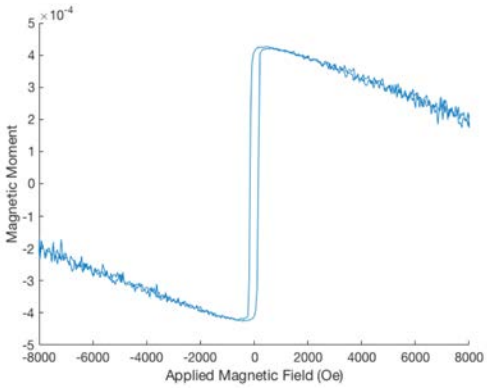

Figure 14: Uncorrected M vs. H hysteresis loop for an Fe_xGa_{1-x} thin film on PIN-PMN-PT measured in the $\langle 110 \rangle$ direction.

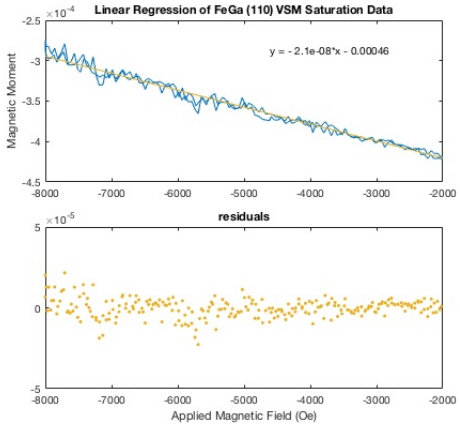

Figure 15: Linear regression on the lower tail of $\langle 110 \rangle$ uncorrected data. Residuals show random scatter indicating that the linear model is valid. The slope of the equation in the upper graph was used as the slope of the linear diamagnetic signal subtracted from the raw data.

The diamagnetic signal from the substrate is characteristically a negatively sloped straight line. The slope of this line was determined via regression on the tails of the uncorrected hysteresis loop (Fig. 15). The result was subtracted from the data. To quantify the magnetic moment in emu/cm^3, the data was divided by the volume of the Fe_xGa_{1-x} film, resulting in the final hysteresis loop used to describe the ferromagnetic properties of the film.

Molecular Beam Epitaxy

The samples in this study were grown by reactive-oxide molecular beam epitaxy (MBE) using a Veeco Gen 10 growth chamber. My graduate student mentor, Rachel Steinhardt, grew all of the films characterized here because the complex method of MBE was beyond the scope of a ten week fellowship. In MBE, pure samples of each element within the desired structure is heated within a crucible, called an effusion cell, to produce a 'beam' that is directed towards the heated substrate. The elements are deposited on the substrate, producing an epitaxial crystalline film. By varying each element's flux rate, substrate temperature, and the pressure of O_2 and ozone within the growth chamber, complex and atomically ordered crystalline films can be grown with high precision.

In order to grow high quality epitaxial crystals, the films must be grown on structurally compatible substrates. For example, lutetium ferrite has a hexagonal structure, rather than the cubic structure of many perovskites grown with MBE. Yttria-stabilized zirconium (YSZ) has a cubic structure that is generally incompatible with the hexagonal ferrites. Yet, when cut to expose the (111) crystallographic plane, the surface behaves hexagonally (Fig. 16). Therefore YSZ (111) is a suitable substrate for lutetium ferrite superlattice growth.

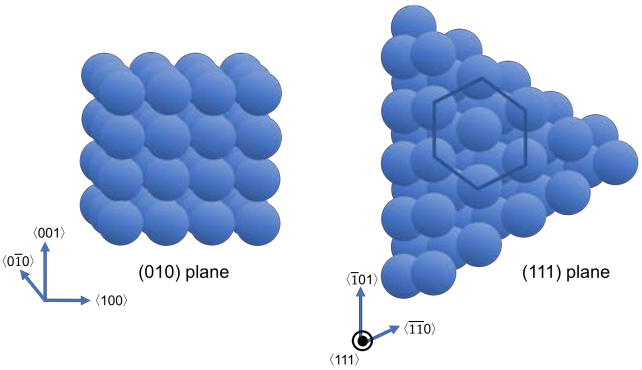

Figure 16: On the left is a simple cubic crystal structure. When sliced to expose the (111) plane, the result is a hexagonal structured surface as depicted on the right. A similar hexagonal structure is produced along the (111) of a face-centered cubic crystal like YSZ. Crystallographic directions are shown for reference.

Acknowledgments

This work was supported by by the National Science Foundation (Platform for the Accelerated Realization, Analysis, and Discovery of Interface Materials (PARADIM)) under Cooperative Agreement No. DMR-1539918 and made use of the Cornell Center for Materials Research Shared Facilities which are supported through the NSF MRSEC program (DMR-1120296). I would like to thank Professor Darrell Schlom for his advice and kindness during this research experience. Special thanks to Rachel Steinhardt for her technical guidance and dedication to making my summer a success. I would also like to thank Professor Katherine Faber for agreeing to act as my faculty co-mentor at Caltech. Finally, I would like to thank the Caltech Student-Faculty Programs office for the opportunity to participate in the Summer Undergraduate Research Fellowship and all of the personnel at both Caltech and Cornell that offered welcome advice and assistance in my voyage across the country to have this world-class research fellowship.

References

[1] Erenstein, W., et al. "Multiferroic and Magnetoelectric Materials." *Nature Reviews* 442 (2006): 759-65.

[2] Martin, L., and D. Schlom. Advanced Synthesis Techniques and Routes to New Single-Phase Multiferroics. *Current Opinion in Solid State and Materials Science* 16.5 (2012): 199215. Web.

[3] Roy, K., et al. "Hybrid Spintronics and Straintronics: A Magnetic Technology for Ultra Low Energy Computing and Signal Processing." *Applied Physics Letters* 99.063108 (2011): n. pag.

[4] Mundy, J., et al. "Atomically Engineered Ferroic Layers Yield a Room-temperature Magnetoelectric Multiferroic." *Nature* 537.7621 (2016): 523-27. Web.

[5] O'Handley, R. *Modern Magnetic Materials: Principles and Applications*. New York, J. Wiley, 2000. Print.

[6] Wang, J., et al. Epitaxial $BiFeO_3$ Multiferroic Thin Film Heterostructures. *Science* 299.5613(2003): 17191722. Web.

[7] Li, Y., et al. "Prediction of Ferroelectricity in $BaTiO_3/SrTiO_3$ Superlattices with Domains." *Applied Physics Letters* 91.11 (2007): 112914.

[8] Fitchorov, T., et al. Tunable Fringe Magnetic Fields Induced by Converse Magnetoelectric Coupling in a FeGa/PMN-PT Multiferroic Heterostructure. *Journal of Applied Physics* 110.12 (2011): 123916. Web.

[9] Niermann, D., et al. "Dielectric properties of charge-ordered $LuFe_2O_4$ revisited: the apparent influence of contacts." *Phys. Rev. Lett.* 109.1 (2012): 016405.

[10] Brooks, C., et al. The Adsorption-Controlled Growth of $LuFe_2O_4$ by Molecular-Beam Epitaxy. *Applied Physics Letters* 101.13 (2012): 132907. Web.